International Journal of Thermofluids 27 (2025) 101272

Contents lists available at ScienceDirect

International Journal of Thermofluids

journal homepage: www.sciencedirect.com/journal/international-journal-of-thermofluids

Enhancing solar chimney performance via tangential partition walls: a computational study

Muhammad Ahmad, Siddique Mohd Umair, Mohammad O. Hamdan *

Mechanical Engineering Department, American University of Sharjah, Sharjah, United Arab Emirates

ARTICLE INFO

Keywords:
Tangential partition walls
Solar chimney
Solar updraft towers
Solar power

ABSTRACT

This study investigates clean energy generation through the efficient utilization of solar irradiance in a solar chimney (SC) system. To overcome the limitations of low airflow rates in conventional designs, tangential partition walls (TPWs) are introduced in the collector section to induce a swirling motion, thereby enhancing airflow and thermal performance. A three-dimensional computational model was developed using ANSYS FLUENT and validated against experimental data from a solar chimney located in Al Ain, UAE. The model was used to analyze flow behavior and assess the average velocity and temperature at the chimney inlet. Results show that TPWs significantly impact SC performance. A configuration with 3 TPWs demonstrated marked improvements in flow velocity and temperature uniformity compared to the baseline design without TPWs. Further enhancement was observed with additional TPWs: a system with 8 TPWs, a 100 m^2 collector area, and a 0.24 m chimney entrance diameter yielded a 350 % increase in kinetic energy. These improvements are attributed to the swirling flow generated near the chimney entrance, which promotes a coherent updraft and reduces recirculation zones. The findings confirm that TPWs offer a promising strategy to boost SC efficiency and support scalable clean energy solutions.

1. Introduction

The UAE has recognized the importance of clean energy and its numerous benefits for sustainable development [1]. Clean energy production, efficient energy conversion, and zero emissions are becoming key drivers of safe and sustainable investments across UAE's emerging energy sector [2]. Over the last decade, clean energy has gained a significant attention worldwide [3].

Among the various renewable energy technologies, solar chimney power plants (SCPPs) offer a promising solution for generating environmentally friendly electricity from solar irradiance [4]. The Manzanares solar chimney power plant in Spain, operational from 1982 to 1989, was the world's first bench mark prototype in solar updraft tower prototype, with a rated power output of 50 kW [5]. In 2004, prototype testing based on the Manzanares design (50 kW output, 195 m chimney height, and a 46,000 m^2 collector area) validated its operational efficiency, demonstrating a 94 % reduction in greenhouse gas emissions compared to conventional coal-fired power plants [4]. Solar chimneys (SCs) have been recognized as an effective approach for passive heating, cooling and ventilation, commercial and domestic purposes. SCs represent an artistic way of clean engineering [6] and considered as a green commercial products [7]. The geological diversity and year-round climatic conditions inspire their customized-hybrid operation. Recent advancements in computational techniques for analyzing SCs have gained a significant attention in the clean energy sector [8–10]. The optimization of SCs is essential to fully utilize solar energy under optimal conditions and reduce investment costs. A solar chimney primarily comprises two main components: the collector and chimney. On the other hand, a solar chimney power plant includes a turbine, which is placed at the chimney entrance to effectively harness the flow potential and generate power.

The design, geometry, material, and surrounding environmental conditions of the SC affect the overall performance of the system [11]. The convective airflow within the SC is highly influenced by geometric parameters. Kasaeian et al. [11] highlighted the importance of air temperature and chimney height in determining the system's output power. Pasumarthi and Sherif [12] reported the dependency of chimney height on entrance airflow rate for day-round operation. The efficiency are observed to be higher during peak hours of solar radiation [12]. Bernardes et al. [13] examined the effect of inlet area, chimney diameter, and height on thermal performance and reported that conical

* Corresponding author.
E-mail address: mhamdan@aus.edu (M.O. Hamdan).

https://doi.org/10.1016/j.ijft.2025.101272

Available online 26 May 2025
2666-2027/© 2025 The Authors. Published by Elsevier Ltd. This is an open access article under the CC BY license (http://creativecommons.org/licenses/by/4.0/).

Nomenclature

A	chimney cross-sectional area [m^2]
D_c	diameter of collector [m]
D	diameter of the chimney [m]
$\dot{E}$	wind kinetic energy [kW]
g	gravitational acceleration [m/s^2]
GW	guide wall
h	convection coefficient [$W/(m^2.K)$]
H	chimney height [m]
k	turbulent kinetic energy [m^2/s^2]
$\dot{m}$	mass flow rate [kg/s]
P	pressure [Pa]
$\dot{q}$	solar heat flux [W/m^2]
SC	Solar Chimney
SCPP	Solar Chimney Power Plant
T	temperature [°C]
TPW	tangential partition wall
u	velocity [m/s]
V	average velocity [m/s]
$\dot{W}$	mechanical power output [kW]
x	coordinate

Greek symbols

α	thermal diffusivity [m^2/s]
ε	turbulence dissipation rate [m^2/s^3]
η	efficiency [-]
μ	dynamic viscosity [Pa·s]
μ_t	turbulent eddy viscosity [Pa·s]
ρ	air density [kg/m^3]

Subscripts

c	collector
i	first index counter
i	second index counter

chimneys exhibit superior performance compared to straight junctions. According to Dai et al. [14], small-scale systems are expected to show faster improvements in system performance with dimensional modifications compared to large-scale systems. In a compact SCPP, the primary force, driving the airflow is buoyancy. This buoyancy effect arises due to the temperature difference between the heated air inside the chimney and the cooler ambient air [14]. This upward draft is crucial for driving the turbine and generating electricity. Pretorius [15] proposed an optimal entrance diameter to improve the efficiency of SCPPs with multi-layer rooftop designs. The multiple-layer rooftop was adopted to describe the multilayer greenhouse collector proposed for thermal energy storage during nighttime operation [15]. Shahreza and Imani [16] proposed a solar chimney design incorporating an air tank and two mirror intensifiers for improved ventilation purposes.

During the early 1980s, Haaf [17] conducted a series of experiments and numerical studies on a pilot plant to evaluate the overall performance of a complete SCPP system.. With an irradiance of 1000 W/m^2, an average velocity of 15 m/s at the entrance of the chimney was observed. According to Haaf [17], the height of the chimney is a critical factor in determining the overall performance of SCPPs for day-round operation. Mullett [18] investigated the effect of SCs for different chimney heights. Zhou et al. [19] investigated the optimal vertical height for the Manzanares prototype as 615 m. The study reported that larger SC designs can potentially achieve higher power output and efficiency by increasing the collector radius and chimney height. In addition, the study reported that both the maximum convection height and the optimal height for maximum power output increase with the collector radius.

Choi et al. [20] proposed a mathematical model to assess the impact of geometric parameters and ground heat storage on SC performance. The presence of a ground heat storage medium is observed to decrease power production during the daytime and produce heating effects after sunset. The continuous variation in climatic conditions, coupled with the potential of geothermal reservoirs, offers a promising avenue for developing sustainable and efficient SCPP [21]. Tingzhen et al. [22] reported the effects of collector diameter, chimney height, solar radiation, and other environmental factors on plant performance and rated power production.

The guide wall (GW) is one of the crucial components held for increasing power production in small-scale designs [23]. A comparative study of airflow with and without GWs was first reported by Kirstein [24]. The study highlighted the importance of design when building the collector-to-chimney transition section. These GWs generate a swirling motion and streamline the airflow with turbine blades at the entrance, resulting in higher net velocity [24]. The use of GWs enhances the rotational kinetic energy of turbine blades at the entrance region. The addition of GWs near the chimney entrance has a strong effect on altering airflow behavior. Elsayed et al. [25] reported that integrating swirl guide vanes (SGVs) into the collector can significantly increase the kinetic energy of the air entering the chimney, leading to higher power output. Ming et al. [26] incorporated radial partition walls (RPWs) in a solar updraft power plant, and reported an enhanced performance. The enhancement is attributed to crosswinds conditions.

Recent developments in SCPPs is focused towards optimizing geometric parameters to enhance efficiency and power output. In this context, divergent chimney designs and chimney heights are massively looked upon by various researchers across the globe. For instance, experimental work on divergent SCPPs demonstrated that increasing chimney height from 4 m to 8 m improves turbine output power by 252 % [27]. The enhancement is attributed to the buoyancy-driven airflow [27]. Further Cuce et al. [28] justified a 0.6° collector slope and 1.5° chimney **divergence angle** as an optimized value for maximum power production. A Divergent chimney-SCPP with sloping collector (DISCPP) outperformance in presence of additional heat source to ground [29]. A new design incorporating the concept of divergent chimney and collector angle with an enhanced volumetric efficiency of 40 % was introduced by [30]. Additionally, parametric studies on semi-elliptical collector designs (e.g., models with 0.01–0.03 m semi-minor heights) revealed performance variations tied to flow dynamics, emphasizing the role of collector curvature in optimizing updraft velocity [31].

Based on the current literature survey, limited work is available in performance investigation of SCPP with use of TPWs. In the current work, the exclusive effect of such TPWs is analyzed using 3-D CFD simulations conducted in FLUENT (ANSYS 2023R2). In context of TPWs [26], investigated the impact of tangentially arranged TPWs on chimney performance, while the current work exclusively classifies the performance metric by observing the velocity and temperature distribution profiles. Simulations are carried out for day-round effects. In this study, numerical simulations are carried out to analyze airflow behavior with TPWs installed in the collector, directing airflow tangentially into the chimney base. Four cases of TPWs and chimney diameter are analyzed. The turbulence effects are captured using velocity streamlines and temperature contours. The study evaluates how TPWs influence airflow rate, power output, and average temperature. Additionally, it examines the effect of chimney diameter on the intensity of the generated swirling airflow, while maintaining other design parameters constant. The proposed design is prototype, and its large-scale implementation may result in higher turbulence palpitation of flow stream, favoring its overall

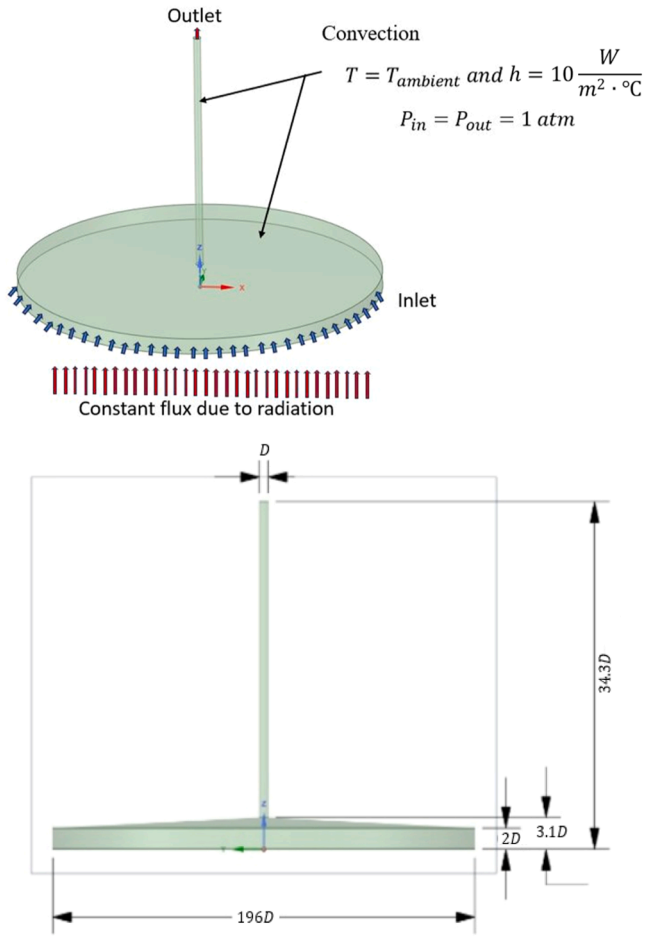


Fig. 1. Schematic diagram of solar chimney system's CFD model.

Table 1
The experimental data for solar heat flux and ambient temperature that has been recorded on December 2nd, 2011, [32].

Time	Ambient temperature °C	Solar heat flux ($\dot{q}$) W/m^2	Velocity measured at chimney entrance m/s
10:00 AM	**20.0**	**222**	**2.9**
11:00 AM	**21.8**	**340**	**3.3**
12:00 PM	**23.4**	**402**	**3.4**
1:00 PM	**25.0**	**474**	**3.3**
2:00 PM	**27.8**	**365**	**3.2**
3:00 PM	**29.2**	**178**	**3.0**

Table 2
Dimensions of solar chimney [34].

Gematric parameters	Units	Range
Diameter of the chimney (***D***)	m	**0.24, 0.36, 0.54 and 0.81**
Height of the chimney (***H***)	m	**8.25**
Diameter of the collector (D_c)	m	**11.3**
Number of tangential partition wall	–	**0, 3, 4, 8**

performance.

2. Problem formulation

A schematic diagram of the computational domain, along with the adopted boundary conditions and dimensions, is shown in Fig. 1. The dimensions of computational domain are in accordance the existing prototype at Al-Ain University, UAE [32]. Chimney's dimensions and boundary values are listed in Tables 1 and 2, **respectively.** The arrangements of different tangential partition walls (TPWs) are illustrated in Fig. 2. These TPWs force the airflow to enter the chimney tangentially, as shown in the close-up image in Fig. 2. Simulations using FLUENT are carried out under the assumption of quasi-equilibrium conditions for a given solar irradiance and ambient temperature for different numbers of TPWs and chimney diameters. A quasi-equilibrium assumption describes a system that is not in complete equilibrium but changes slowly enough to be considered as a series of steady equilibrium states. The numerical results are first validated with the existing prototype. The material used to form the SC has low specific thermal capacity, and the ground is modeled as a boundary representing constant heat flux. The performance of the SC for day-round operation is modeled by applying a time-dependent variable heat flux, as per the previous experimental results of [34].

The steady-state numerical simulations are performed with a standard $k-\varepsilon$ turbulence model. The Boussinesq approximation is applied to account for buoyancy-driven flow caused by density variations. Ambient temperatures for specific solar heat flux, as per the previous experimental results, are reported in Table 1 [34]. The experimental study was carried out for day-round operation on December 2, 2011, by [34], in Al Ain, UAE. In summary, the following assumptions are applied for the present simulation of the SC:

1. Given the moderate flow velocities (Mach < 0.3), the airflow within the chimney is modeled as steady and incompressible, consistent with standard buoyancy-driven flow assumptions [32].
2. Natural convection with a heat transfer rate of 10 W/m^2·K [35] is applied at the collector and chimney surface. However, an accurate consideration of solar irradiance depends on the collector's efficiency and its inclination.
3. The boundary values of solar heat flux and ambient temperature for day-round operation, obtained from the previous experimental study, are simulated as per Table 2 [32,34,35].
4. Gravity is set at -9.81 m/s^2.
5. The inlet and outlet pressures are considered constant (1 atm) for such a short-height chimney (as shown in Table 3), and simulations are modeled for zero wind velocity neglecting the ground effect.

3. Numerical solution

The numerical simulations explore four different TPWs configurations and four chimney diameters. The baseline configuration, representing an experimental solar chimney design [34], consists of zero TPWs, a chimney height of 8.25 m, and a diameter of 0.24 m. The numerical simulation of the flow through the solar chimney with TPWs is conducted using FLUENT. Both configurations without and with TPWs are simulated to highlight the relative variance in the system potential, imposing the boundary conditions listed in Table 1.

3.1. Governing equations

The current solar chimney design is simulated using FLUENT of commercial ANSYS pack (2023) under zero wind speed and unloaded condition (turbine). Based on previous literature review, the standard $\boldsymbol{k-\varepsilon}$ turbulence model is selected for predicting the flow behavior inside the chimney, [13,32,36]. Based on the assumption made, the simplified governing equations and turbulence model are given in Eqs. (1–3). Eq.

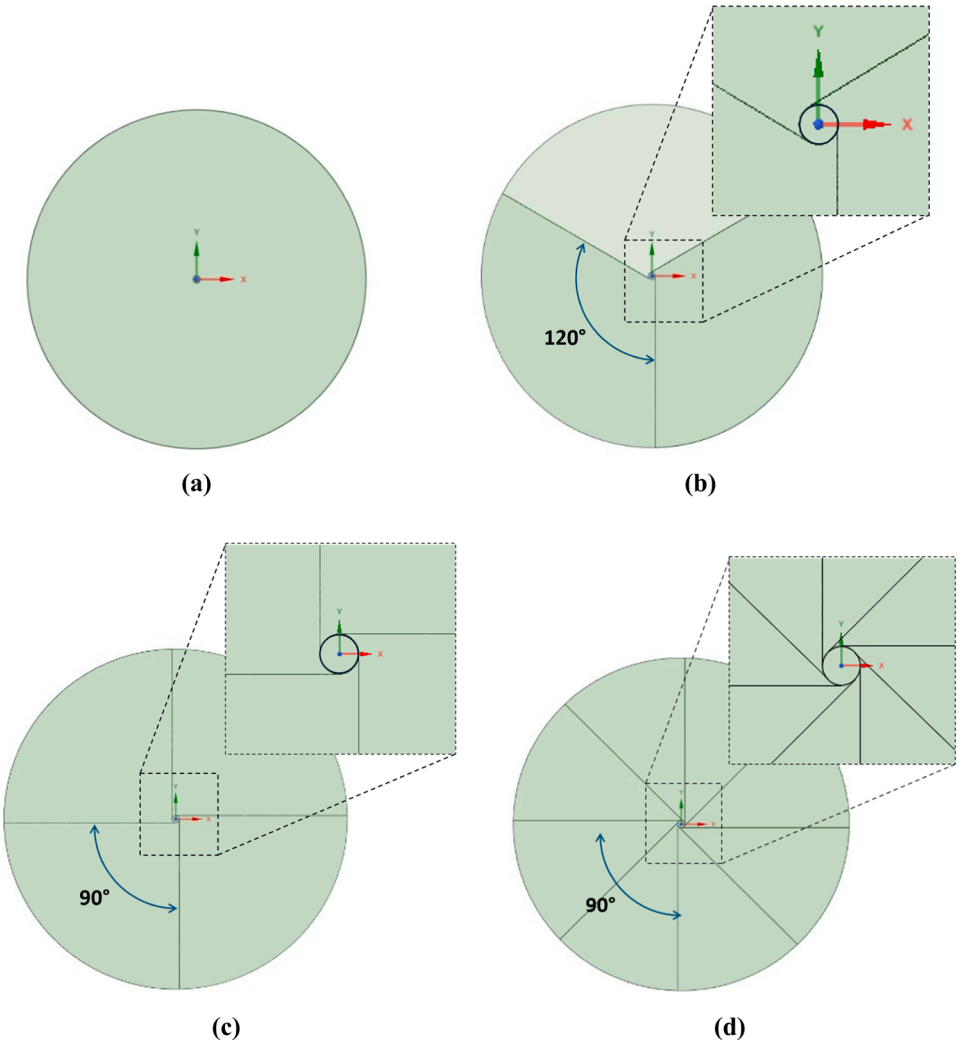


Fig. 2. Schematic top-view of the collector for four configurations with a close-up view of the connection between collector and chimney for (a) 0 TPWs (baseline configuration), (b) 3 TPWs, (c) 4 TPWs, and (d) 8 TPWs.

Table 3
Boundary condition of computational domain [32].

Boundary parameters	Units	Range
Convection coefficient (***h***)	W/(m^2°C)	**10**
Pressure at inlet and outlet	atm	**1**
Heat Flux	W/m^2	**222–178**
Inlet temperature	°C	**20–29.2**

(1) represents the mass conservation continuity equation in the ***x, y***, and ***z*** directions, where the subscript (*i*) denotes the respective direction [13, 37]. A traditional model of mass momentum conservation model is incorporated for present simulation in line with previous work of [13, 38]. The energy equation is modelled for predicting a varying temperature incorporating the Boussinesq approximation effect of density driven flow, [13,37].

Conservation of mass

$$\frac{\partial u_i}{\partial x_i} = 0 \tag{1}$$

Conservation of momentum

$$\rho u_i \frac{\partial y}{\partial x} = -\frac{\partial P}{\partial x_i} - \rho g_i - \frac{\partial}{\partial x_i}\left[\mu\left(\frac{\partial u_i}{\partial x_i} + \frac{\partial u_i}{\partial x_i}\right) - \rho\overline{u_i' u_j'}\right] \tag{2}$$

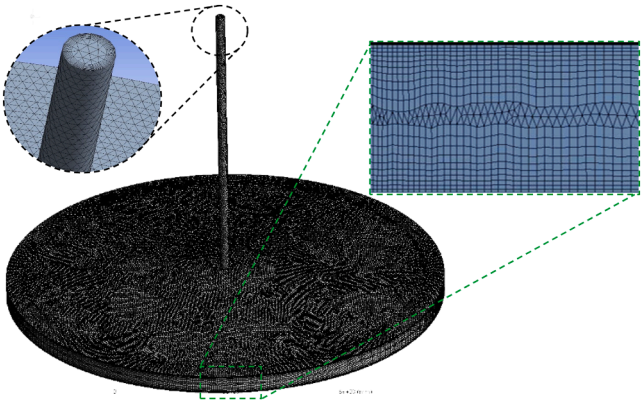


Fig. 3. A tetrahedron mesh structure of the computational domain.

Conservation of energy

$$u_i \frac{\partial T_i}{\partial x_j} = \frac{\partial}{\partial x_i}\left[\alpha \frac{\partial T}{\partial x_j} - \overline{T' u_j'}\right] \tag{3}$$

The Reynolds stresses ($-\rho\overline{u_i' u_j'}$) are calculated using the standard $k-\varepsilon$ model for high Reynolds numbers [39,40]. A wall function is

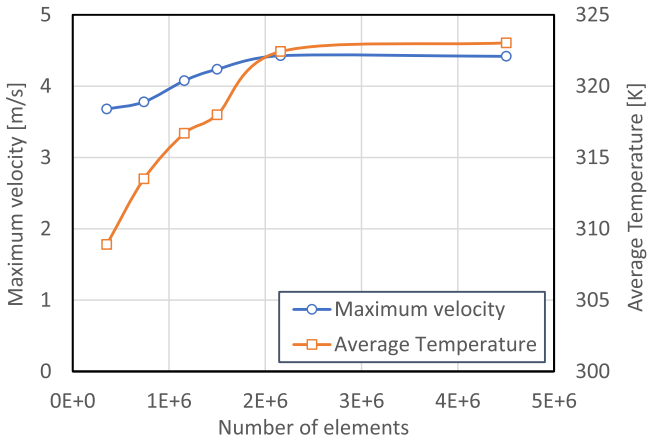


Fig. 4. Grid independence study with the used number of grid elements.

implemented to account for the phenomenon occurring close to boundary layer. The turbulent kinetic energy (k) and the dissipation rate of kinetic energy (ε) are solved through the following transport equations:

$$k = \frac{\overline{u_i' u_i'}}{2} \tag{4}$$

$$\varepsilon = \left(\frac{\mu}{\rho}\right)\left(\frac{\partial u_i'}{\partial x_j}\right)\left(\frac{\partial u_j'}{\partial x_i}\right) \tag{5}$$

$$\rho u_j \frac{\partial k}{\partial x_j} = \frac{\partial}{\partial x_j}\left[\left(\mu + \frac{\mu_t}{\sigma_k}\right)\frac{\partial k}{\partial k_j}\right] + P_k - \rho\varepsilon \tag{6}$$

$$\rho u_j \frac{\partial \varepsilon}{\partial x_j} = \frac{\partial}{\partial x_j}\left[\left(\mu + \frac{\mu_t}{\sigma_\varepsilon}\right)\frac{\partial \varepsilon}{\partial k_j}\right] + C_{1\varepsilon}P_k\frac{\varepsilon}{k} - C_{2\varepsilon}\rho\frac{\varepsilon^2}{k} \tag{7}$$

where, the variables turbulent eddy viscosity (μ_t), production of turbulent kinetic energy(k_p), and turbulent heat flux ($-\rho\overline{T'u_j'}$) are calculated using the Eqs. (8)–(10) correspondingly [40].

$$\mu_t = C_\mu \rho \frac{k^2}{\varepsilon} \tag{8}$$

$$P_k = -\rho\overline{u_i' u_j'}\left(\frac{\partial u_j}{\partial x_i}\right) \tag{9}$$

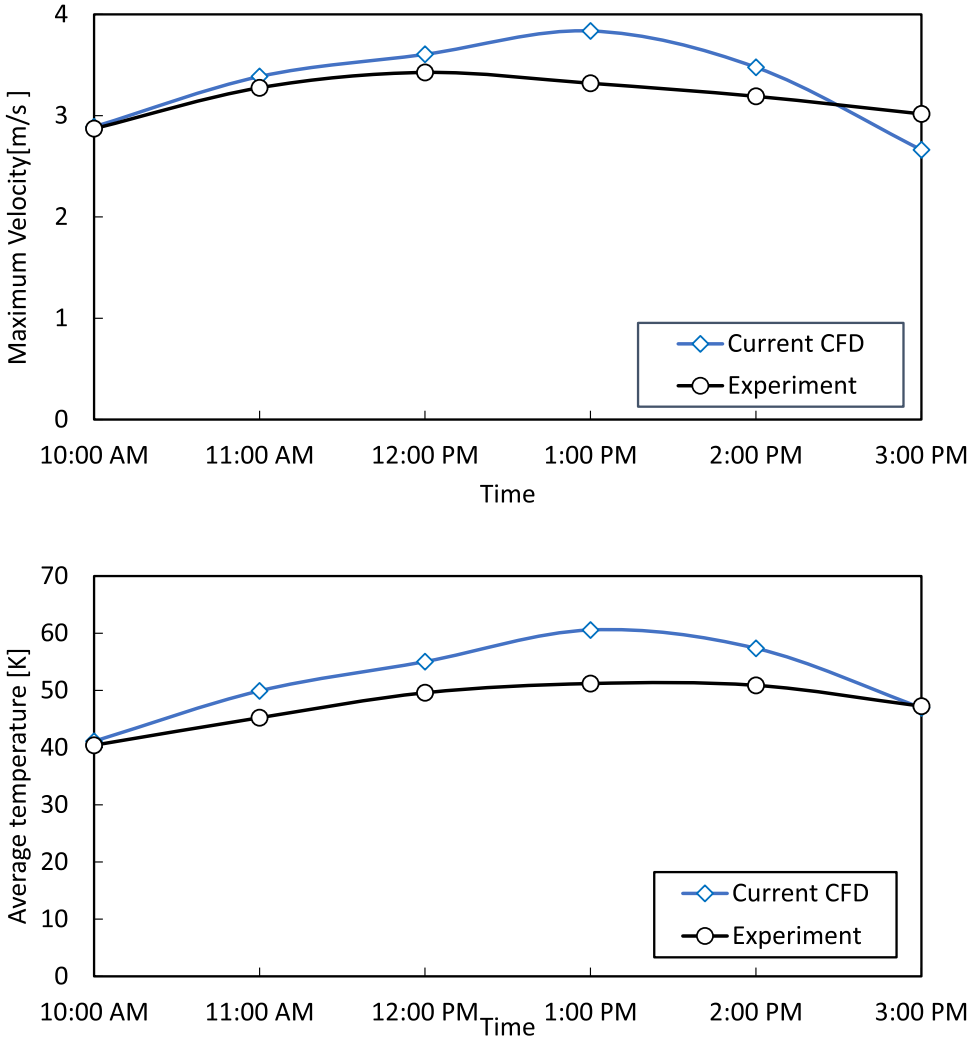


Fig. 5. (a) Maximum velocity (b) Temperature at the entrance of chimneys for different hours of day-round operation from experimental study [34] and current CFD model.

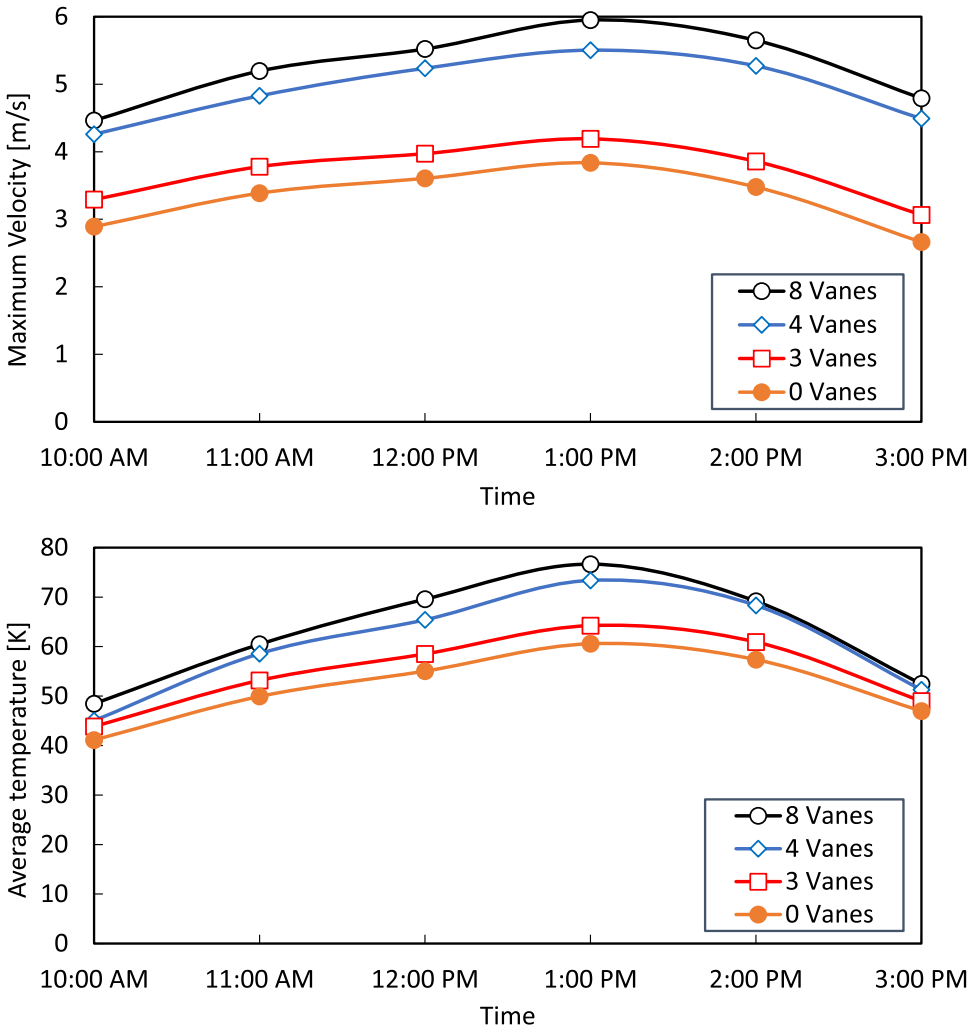


Fig. 6. The maximum velocity (a) and average temperature (b) at the chimney's entrance for 0, 3, 4, and 8 TPWs.

$$\rho\overline{T'u_j'} = \frac{\mu_t}{\sigma_t}\left(\frac{\partial u_j}{\partial x_i}\right) \tag{10}$$

The constants, used in standard $k-\varepsilon$ model, are assigned the following values $\sigma_k = 1$, $\sigma_\varepsilon = 1.3$, $\sigma_T = 0.85$,$C_{1\varepsilon} = 1.44$, $C_{2\varepsilon} = 1.92$, and $C_\mu = 0.09$ [40]. The turbulent Reynolds stress is calculated using Eq. (11).

$$-\rho\overline{u_i'u_j'} = \left[\mu\left(\frac{\partial u_i}{\partial x_j}+\frac{\partial u_j}{\partial x_i}\right)\right] - \frac{2}{3}\rho k\delta_{ij} \tag{11}$$

3.2. Numerical scheme criteria

To ensure the accuracy of the numerical model, a uniform fine tetrahedral grid with inflation near the wall is adopted, Fig. 3. A steady-state pressure base solver has been enforced while an energy model with the turbulent flow has been activated for capturing the convective flow and heat transfer. In this study, the least-squares cell-based approach has been used to solve partial differential governing equations. A second-order upwind scheme for pressure, momentum, and energy has been used. The convergence and residual values were set at 10^{-6} for continuity, and velocity, and 10^{-13} for energy. A hybrid initialization method is opted for current simulation. The simulations are carried out using parametric study of FLUENT, which is basically a multi-run steady-state simulation under different heat fluxes.

3.3. Mesh independence study

A mesh independence study is conducted to ensure that the results are not influenced by grid size or density, as shown in Fig. 4. In this analysis, the chimney's entrance velocity and average temperature are used as evaluative parameters. Based on Fig. 4, a grid size of 2,159,768 elements is found to be optimal.

3.4. Validation study

To assess the accuracy of the numerical solution, a validation study is conducted by comparing the numerical results with experimental data from the literature. As shown in Fig. 5, the CFD results, specifically maximum velocity and average temperature values, are validated against experimental data from a small-scale prototype built in Al Ain, UAE [34]. The prototype was constructed without TPWs features a 100 m^2 collector area, chimney height of 8.25 m and diameter of 0.24 m.

The numerical model is solved under a quasi-equilibrium assumption under different heat flux boundary value. . A quasi-equilibrium assumption is considered appropriate for this study since the system's low heat capacity causes temperature changes to occur more rapidly than variations in solar heat flux, which remains relatively gradual over time.

As shown in Fig. 5, the CFD model accurately predicts the temperature and velocity distribution for varying heat flux condition, within an average error of 6.68 % and 9.35 %, and root mean square error of 7.47

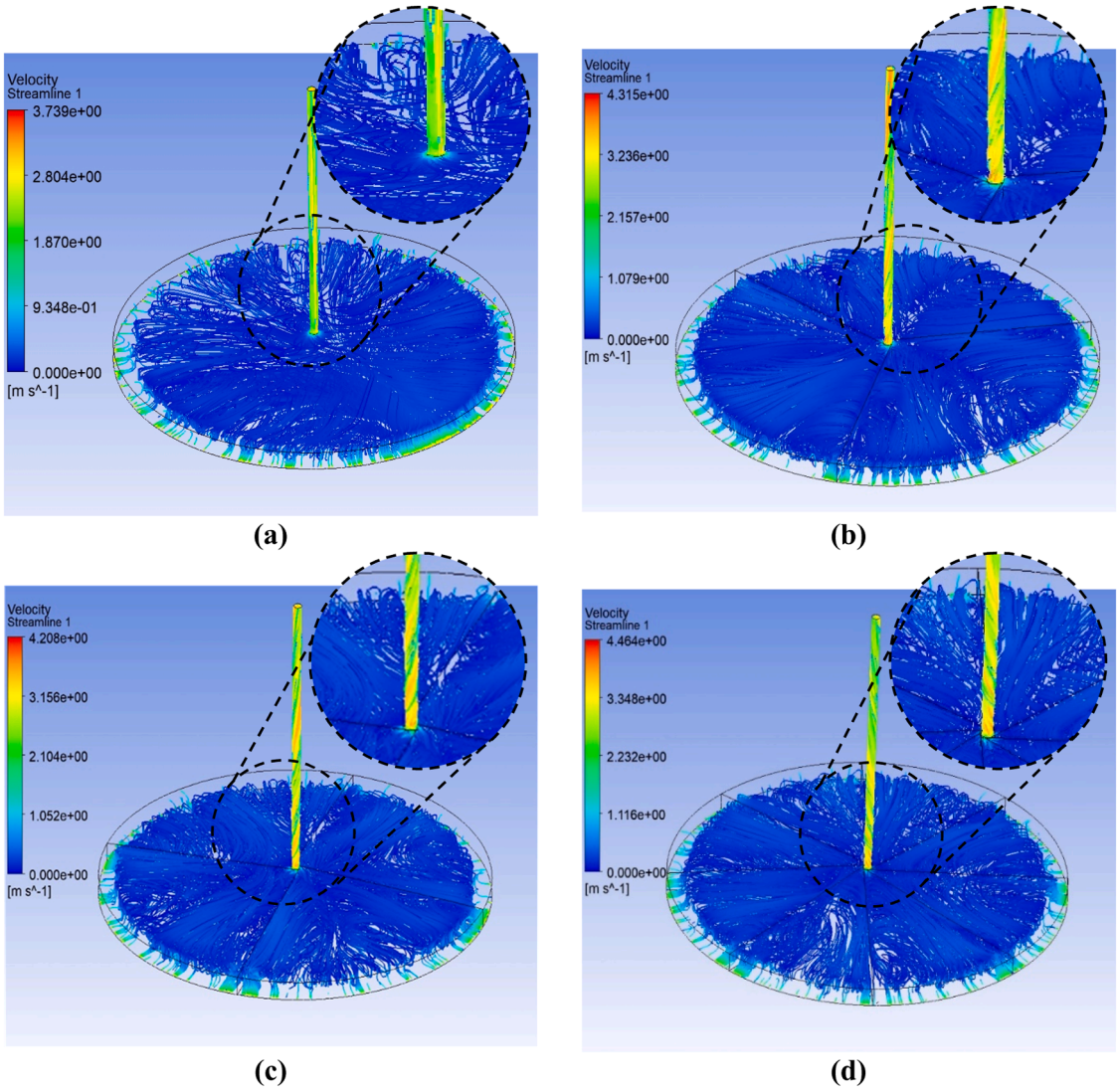


Fig. 7. The velocity streamlines at 1:00 PM, corresponding to a heat flux of 474 W/m^2 and an ambient temperature of 25 °C, are displayed for configurations with (a) 0, (b) 3, (c) 4, and (d) 8 TPWs.

% and 10.65 %, respectively . While the numerical results overestimate the experimental results, it resembles a peak deviation in maximum velocity and average temperature values, particularly at 1 PM, near the chimney entrance.

The transient nature of airflow within the solar chimney, driven by the continuously varying heat flux, presents challenges in achieving precise numerical predictions. Additionally, unaccounted-for external factors, such as wind conditions, [32]. Ground's role as a heat capacity medium contributes to a slight overestimation in velocity and temperature values.

The validated CFD model serves as the baseline configuration for analyzing the impact of TPWs on solar chimney performance.

4. Results and discussion

The study primarily reports the maximum velocity and average temperature at the chimney inlet. Velocity streamlines, and temperature contours are further analyzed and discussed for enhancement in flow rate and power generated.

4.1. Effect of numbers of tangential partition walls

Fig. 6 shows the behavior of maximum velocity and average temperature at the chimney inlet for four cases: 0, 3, 4, and 8 TPWs. The figure is generated by varying the heat flux input as a function of time, as listed in Table 1. As expected, with increasing heat flux, the air temperature inside the collector rises, which in turn enhances the buoyancy-driven flow, causing the fluid to move faster inside the chimney. Consequently, as the solar flux varies periodically throughout the day, both maximum velocity and average temperature exhibit similar variations. These values peak around 1 PM, when the maximum radiation reaches its highest value.

When considering the transient behavior, velocity and temperature would typically lag behind the heat flux, depending on the heat capacity of the solar chimney system. However, as pointed out in this study, the quasi-equilibrium approach is acceptable for predicting the behavior of the solar chimney within an acceptable range due to the system's low heat capacity.

The baseline state serves as a reference for assessing the effects of different TPWs. As shown in Fig. 6a and b, the maximum velocity and average temperature at the chimney inlet increase with the number of TPWs. This is due to the improved flow pattern, which maximizes heat transfer through the collector. The TPWs reduce turbulence in the airflow, improving flow performance and enhancing heat transfer. The addition of TPWs introduces a swirling component to the incoming airflow at the chimney entrance. As the airflow passes through the

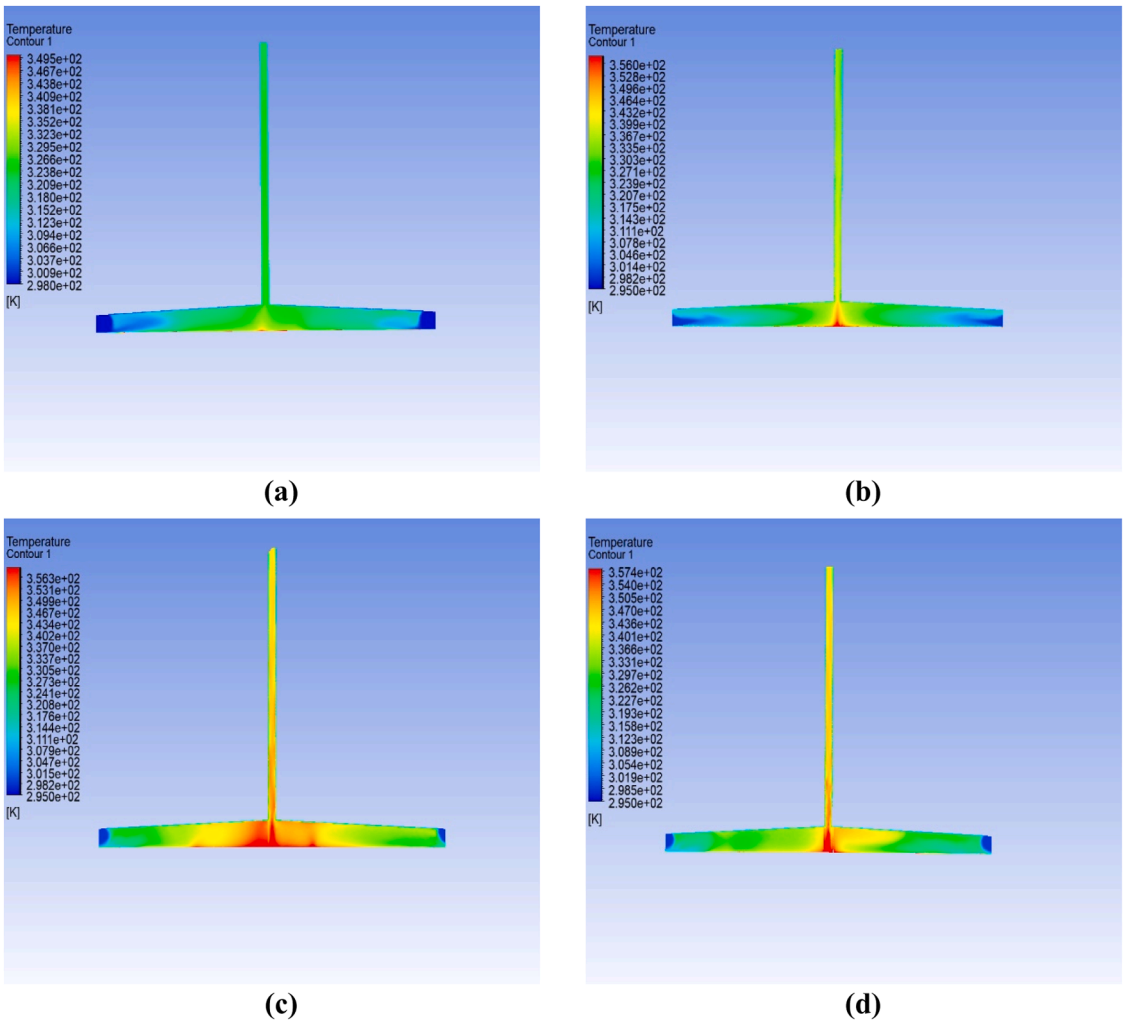


Fig. 8. The temperature contours at 1:00 PM, corresponding to a heat flux of 474 W/m^2 and an ambient temperature of 25 °C, are presented for configurations with (a) 0, (b) 3, (c) 4, and (d) 8 TPWs.

TPWs, it gains tangential velocity, while the radial flow toward the center is limited. Consequently, the addition of TPWs intensifies the swirling motion within the solar chimney, leading to a significantly enhanced heat transfer effectiveness.

To better understand this behavior, it is important to examine the streamlines for these cases. As shown in Fig. 7 with increase in number of TPWs, the flow chaos reduces, and the streamlines become more organized, strengthening the airflow and improving heat transfer. As heat transfer improves, the buoyancy effect is enhanced, further improving the air flow rate. Therefore, under the given simulation conditions, it is expected that the flow rate and average temperature will increase significantly as the number of TPWs increases.

Additionally, the swirling flow exhibits a lower tendency for flow separation compared to conventional axial flows due to the tangential velocity and associated radial pressure gradients. This characteristic ensures the flow remains attached to the chimney wall surfaces. Without a swirling component, the sharp edge of the solar chimney's entrance could induce flow separation in the incoming flow. The TPWs effectively reduce pressure losses caused by significant flow separation at the chimney inlet. This reduction in energy losses at the entrance allows the airflow to accelerate as it enters the chimney. Consequently, the presence of TPWs results in higher maximum air velocity values downstream of the entrance.

Moreover, the swirling elements induced by the tangential speed enhance the turbulence level. The organized swirl stabilizes chaotic flow structures by making the turbulence more uniform or directing it in specific patterns. By integrating TPWs, the combination of reduced pressure losses and increased turbulence improves the maximum airflow velocities within the chimney. Overall, the presence of TPWs favors the creation of stronger coherent updraft, buoyancy driven flow leading to an enhanced air flow rate. Without TPWs the air in the entrance region is more diffuse and may create a recirculation zone. Clear trends emerge in the comparison of different configurations with 0, 3, 4, and 8 TPWs, as shown in Fig. 7.

While peak temperatures may slightly decrease due to improved thermal energy transfer from the hot central flow to the near-wall flow, the maximum temperatures are confined to a narrower range across the chimney diameter. The inclusion of TPWs results in a more uniform profile, eliminating the sharp temperature gradients observed without TPWs. The swirl effect similarly facilitates thermal mixing, contributing to more uniform temperatures deeper into the chimney. Hence, the TPWs enhance thermal mixing, leading to more consistent temperature profiles and improved lateral uniformity both at the solar chimney entrance and downstream areas. The introduction of three TPWs induces a gentle swirling flow, enhancing the dispersion of heat, creating a more focused heat zone near the chimney entrance by reducing the lateral spread. Additionally, the presence of TPWs acts as thermal insulator between the flow sectors, resulting in enhanced room for solar heat utilization. The TPWs also promote the thermal boundary layer development, extending the heat retention time.

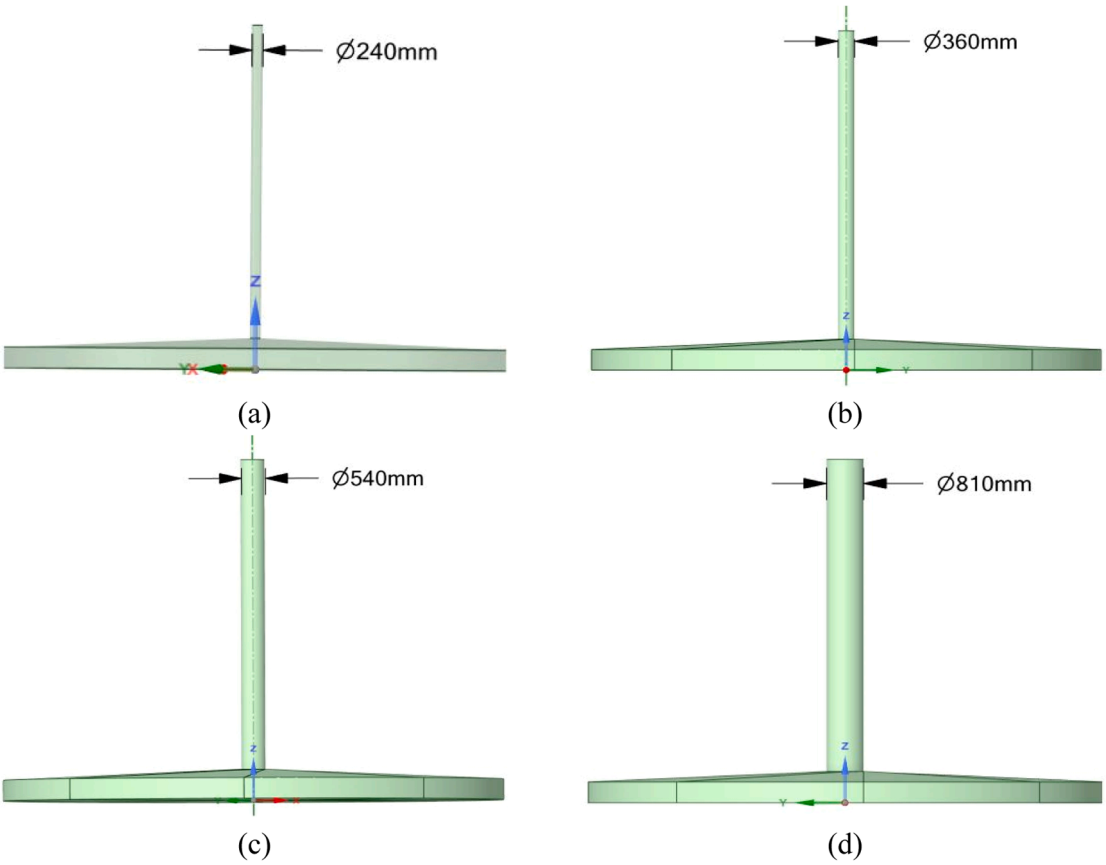


Fig. 9. Different Diameters of Chimney (a) 240 mm (b) 360 mm (c) 540 mm (d) 810 mm.

The significant improvement in velocity at the entrance indicates a greater volume of air being exposed to solar heat. As a result, pressure losses are further reduced through enhanced flow attachment, leading to more effective utilization of solar energy.

Fig. 7a illustrates that the absence of TPWs leads to unorganized airflow, resulting in ineffective heat absorption. The introduction of 3 TPWs induces a gentle swirl, enhancing heat absorption. With 4 TPWs, the swirling motion becomes more pronounced, leading to a significant improvement in heat transfer. These findings underscore the importance of carefully selecting the number of TPWs to achieve a balance between maximizing heat absorption and addressing potential efficiency concerns.

The improved heat transfer results in higher temperatures inside the solar chimney, as shown in Fig. 8. The temperature contour profiles in Fig. 8 demonstrate that as the number of TPWs increases, a more uniform temperature distribution is achieved, signifying improved heat absorption and reduced pressure losses. Additionally, the figure shows that the maximum temperature reached within the SC increases as the number of TPWs increases.

4.2. *Effect of chimney diameters*

The chimney diameter is a crucial design parameter that directly influences airflow patterns and velocities within the system. To maximize energy extraction in a solar chimney, it is essential to optimize the chimney diameter in relation to the collector area. These systems rely on buoyancy-driven airflow induced by solar heating. As reported in the literature by [32], the chimney diameter significantly affects the harvested power, especially when it falls below a critical value. This critical diameter depends on factors such as the Reynolds number and the boundary layer thickness [33]. Once the chimney diameter exceeds the critical value, its impact on harvested power becomes minimal.

This study numerically investigates the impact of different chimney diameters on swirl flow behavior. Schematics of all examined chimney diameters are shown in Fig. 9, with the four different diameters being 240 mm, 360 mm, 540 mm, and 810 mm.

Fig. 10 presents the variation in maximum velocity and average temperature at the chimney inlet for four different chimney diameters: 240, 360, 540, and 810 mm. These results are obtained by altering the heat flux input over time, as detailed in Table 1. As the heat flux increases, the air temperature within the collector rises, which strengthens the buoyancy-driven flow potential and speeds up the airflow through the chimney. Accordingly, as the solar flux changes periodically throughout the day, both maximum velocity and average temperature exhibit corresponding variations, as shown in Fig. 10.

As shown in Fig. 10a, the maximum velocity at the chimney inlet varies throughout the day, closely following the pattern of solar irradiation. During the morning, as solar irradiation increases, the velocity steadily rises, reaching its peak around midday when solar irradiation is at its highest. Smaller chimney diameters, such as ∅240 mm, exhibit significantly higher maximum velocities compared to larger diameters, as the smaller cross-sectional area enhances the buoyancy-driven flow. After midday, the velocity declines consistently across all chimney diameters as solar irradiation decreases. This behavior highlights the direct correlation between solar irradiation and the buoyancy-induced airflow, with smaller diameters showing greater sensitivity to changes in solar heating.

Fig. 10b shows the variation of average temperature at the chimney inlet over the day for the four examined chimney diameters, highlighting a direct relationship with solar irradiation. In the morning, the average temperature rises steadily as solar energy increases, with smaller chimneys, particularly ∅240 mm, exhibiting higher temperatures compared to the rest of the cases. Around midday, when solar irradiation peaks, the average temperature also reaches its maximum,

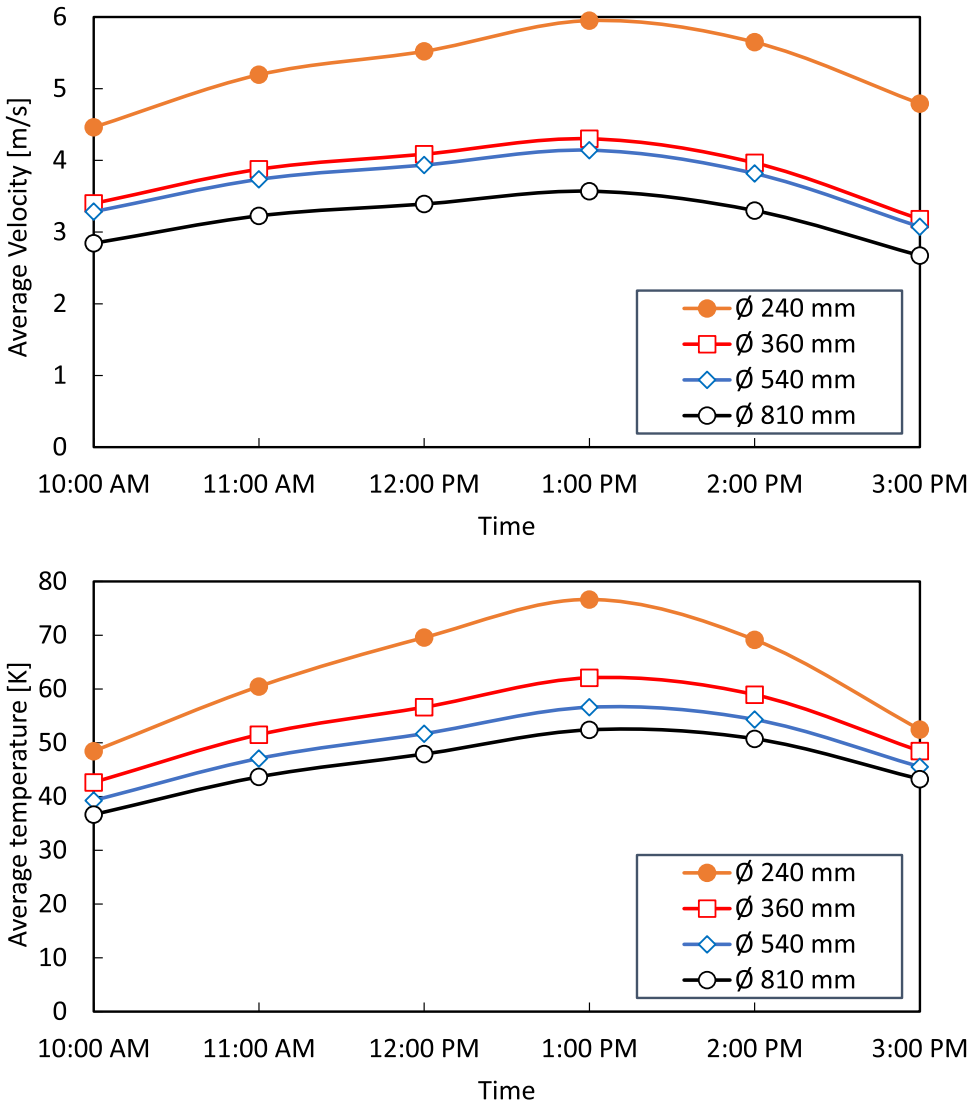


Fig. 10. The variation of (a) maximum velocity and (b) Average temperature for different hours of day-round operation at the chimney's entrance for 8 TPWs and different chimney diameters.

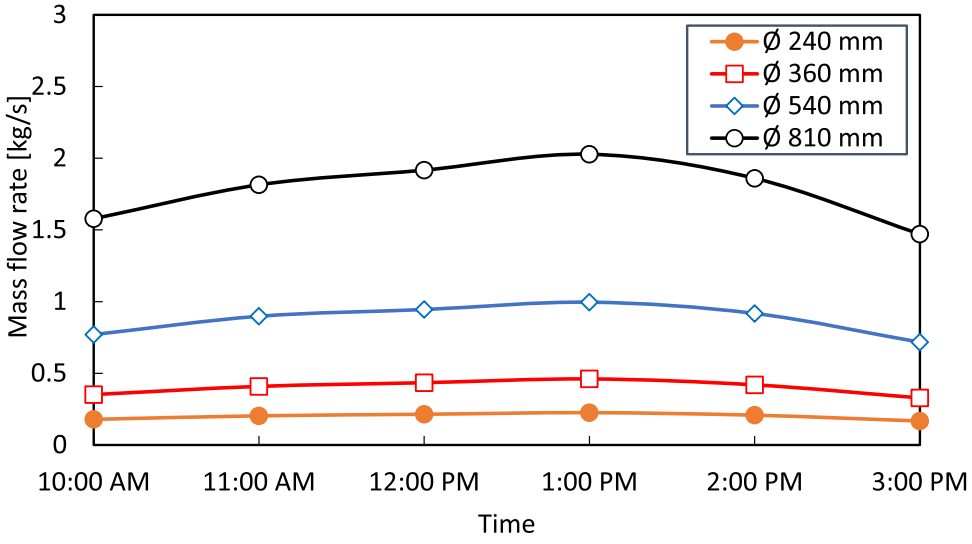


Fig. 11. The variation of mass flow rate for different hours of day-round operation at the chimney's entrance for 8 TPWs and different chimney diameters.

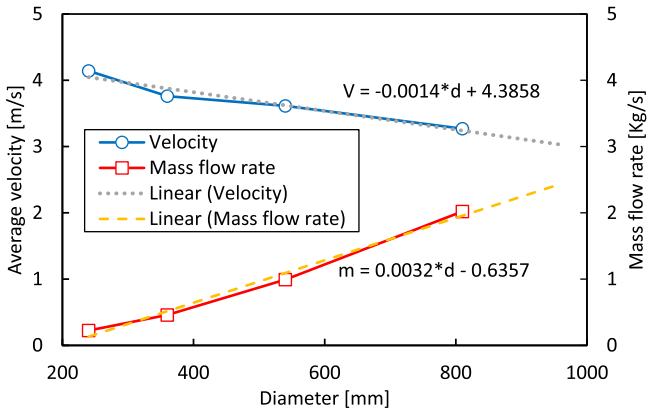


Fig. 12. The variation of (a) average velocity and (b) mass flow rate with chimney diameter for SC with 8 TPWs at 1:00 PM (heat flux of 474 W/m^2 and 25 °C).

with the ∅240 mm chimney maintaining the highest value. In the afternoon, as solar energy declines, the average temperature decreases for all configurations at a similar rate. A smaller chimney diameter consistently results in an increase in mass flow rate and average temperature as compared with higher diameter in presence of TPW. This suggests that a lower mass flow rate is experienced within smaller chimneys. The reduced flow rate is expected, with an increase in diameter due to higher frictional loss associated. To better understand this behavior, it is essential to examine the variation of flow rate over time for different chimney diameters, as shown in Fig. 11, and the variation of average velocity and mass flow rate with chimney diameter at 1:00 PM (heat flux of 474 W/m^2 and 25 °C), as shown in Fig. 12. In these figures, it is evident that the mass flow rate increases with larger chimney diameters, as mass flow rate is related to the square of the diameter. This second-order relationship implies that even small increases in diameter result in a significantly higher flow rate due to reduced friction losses and a greater capacity for airflow. It may seem confusing that the maximum velocity decreases with an increase in diameter while the mass flow rate increases. To clarify these relationships, Fig. 12 presents the variation of average velocity and mass flow rate with chimney diameter for a SCPP operating with 8 TPWs. The data is shown for 1:00 PM under a heat flux of 474 W/m^2 and an ambient temperature of 25 °C. The figure illustrates how changes in chimney diameter influence airflow characteristics, providing insight into the system's performance under these specific conditions. The results representing the characteristic curve for mass flow rate and average velocity are applicable for unloaded conditions. The blue curve represents the average velocity, which decreases linearly as the chimney diameter increases. This behavior can be attributed to the inverse relationship between velocity and cross-sectional area, as a larger diameter reduces the flow speed for a given volumetric flow rate. On the other hand, the red curve illustrates the mass flow rate, which increases linearly with the chimney diameter. This is expected since mass flow rate is directly proportional to the cross-sectional area (square

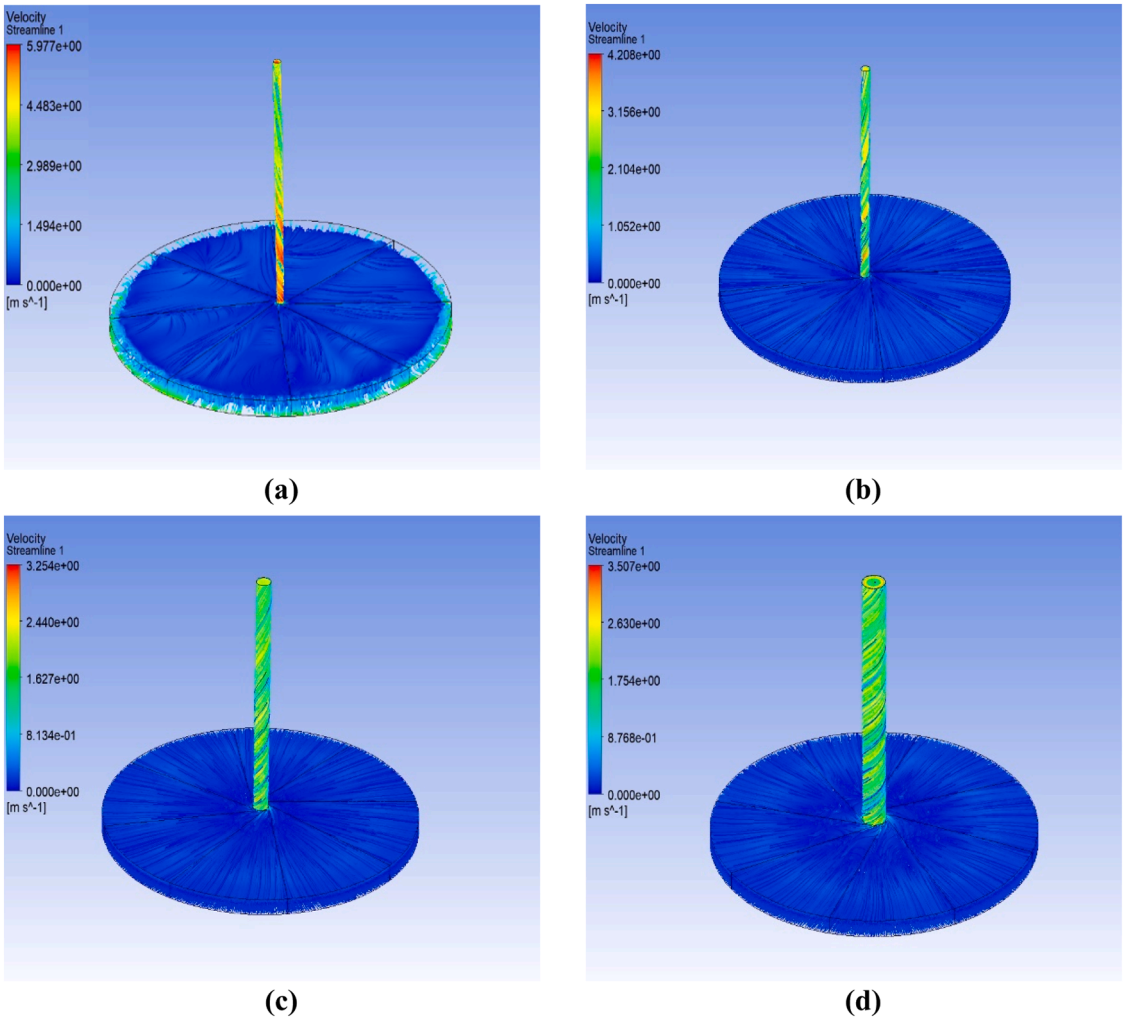


Fig. 13. Velocity contour for different chimney diameters at 1:00 PM (heat flux of 474 W/m^2 and 25 °C) (a) 240 mm (b) 360 mm (c) 540 and (d) 810 mm.

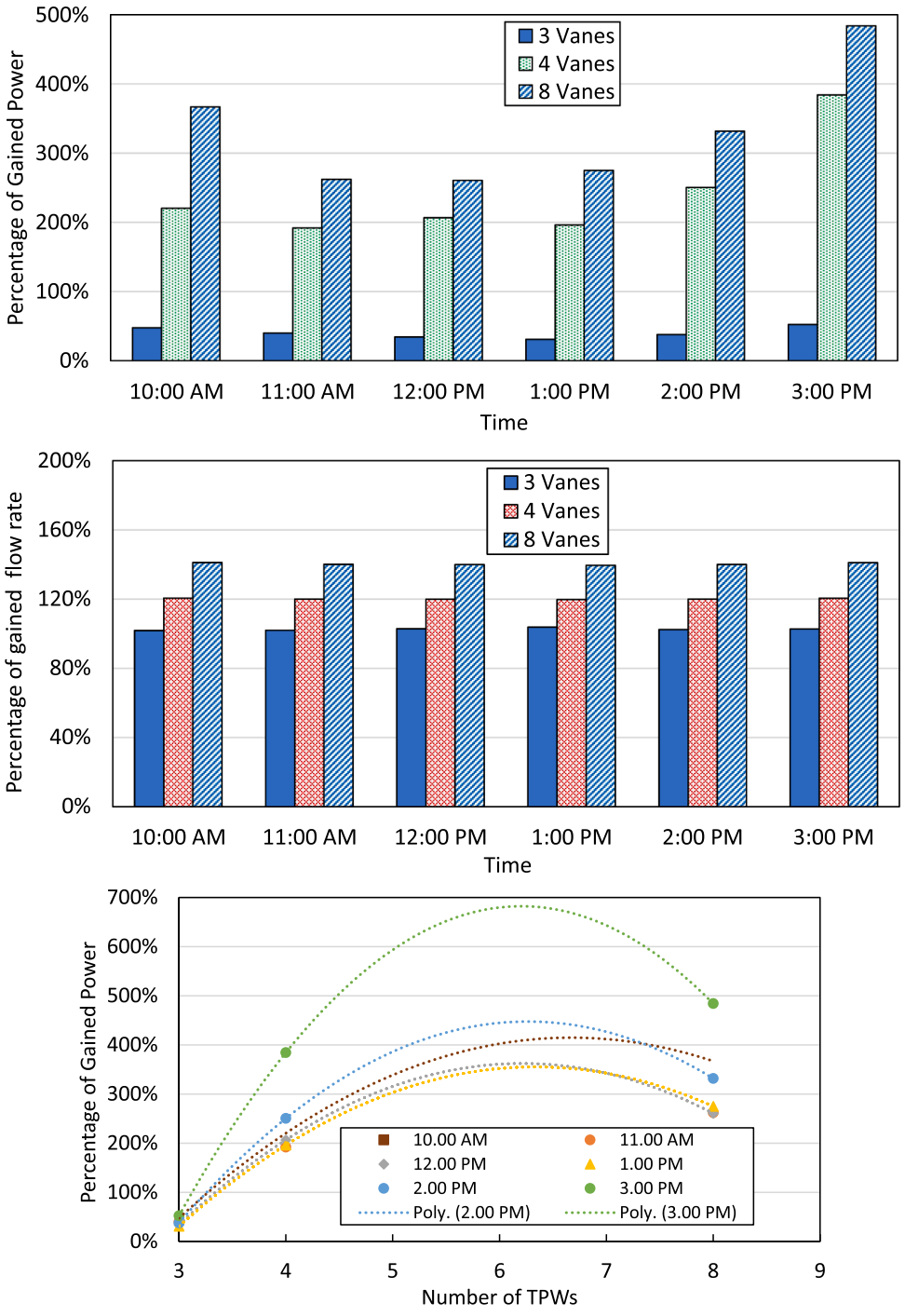


Fig. 14. The variation of (a) percentage of gained power, (b) percentage of gained mass flow rate and (c) percentage of gained power trend for increasing number of TPWs as 3,4 and 8.

of the diameter) and airflow density. The larger diameter facilitates a greater volume of air to flow, despite the reduction in velocity, resulting in a net increase in mass flow rate. The linear trend lines and equations for both velocity and mass flow rate highlight the predictable, contrasting effects of increasing chimney diameter on these two parameters. Overall, the figure underscores the trade-off between velocity and mass flow rate when designing chimney diameters for optimal performance in SC systems.

Fig. 13 illustrates velocity contours and streamlines for chimney diameters of 240 mm, 360 mm, 540 mm and 810 mm, highlighting the impact of chimney size on velocity distribution within a SCPP. For the smallest diameter (240 mm), the velocity is the highest near the chimney inlet, with concentrated streamlines indicating accelerated flow due to a smaller cross-sectional area. As the diameter increases to 360 mm and 540 mm, the velocity decreases, and the contours reveal a broader distribution of lower velocities near the chimney base, attributed to the increased area facilitating higher mass flow rates but reducing flow velocity. For the largest diameter (810 mm), the velocity is the lowest, and the streamlines show a dispersed airflow with greater friction losses. The results demonstrate the trade-off between velocity and chimney diameter: smaller diameters yield higher velocities but lower mass flow rates, while larger diameters reduce velocity but increase mass flow capacity, emphasizing the need to optimize chimney dimensions for performance.

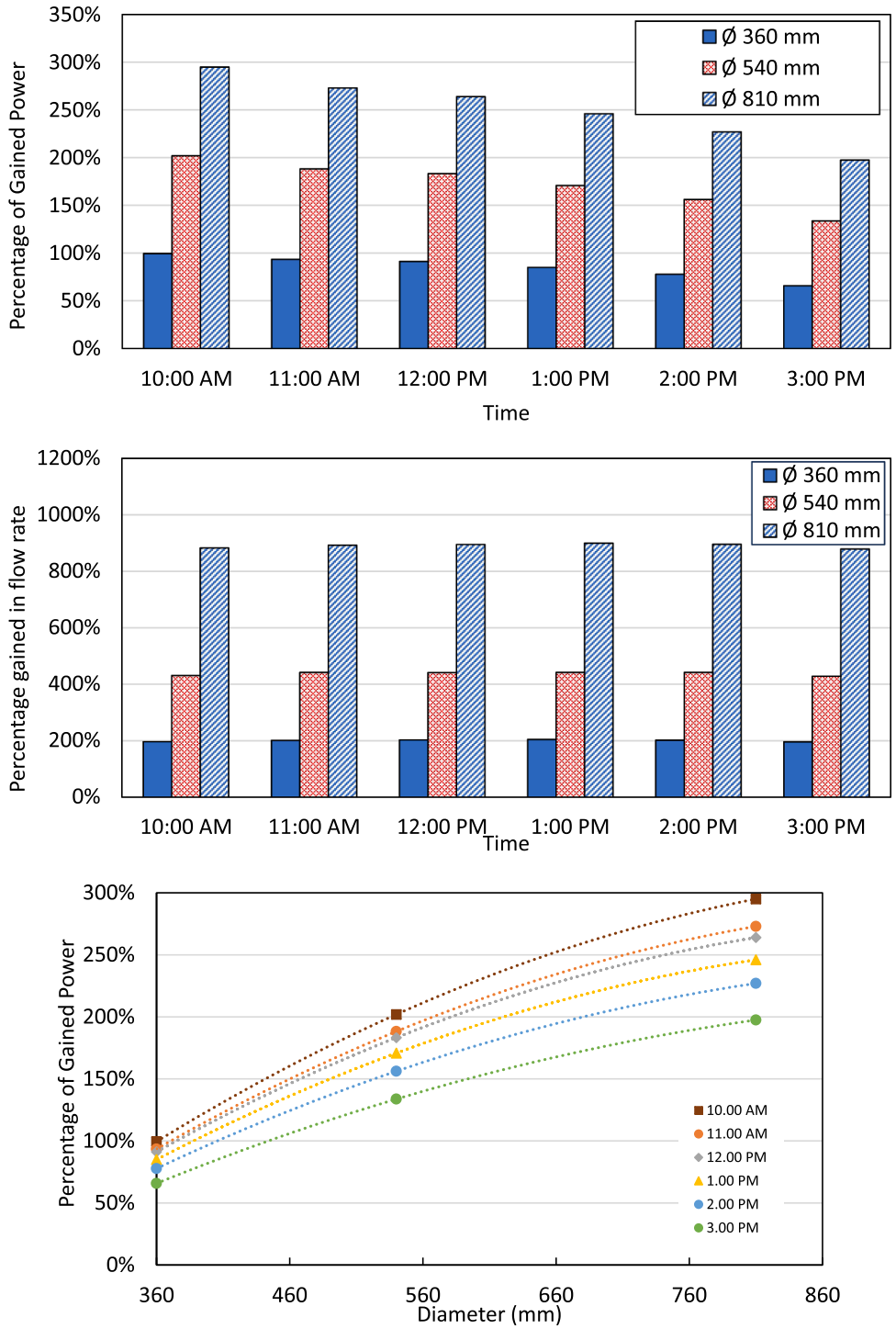


Fig. 15. The variation of (a) percentage of gained power, (b) percentage of gained mass flow rate and (c) percentage of gained power trend for increasing chimney diameter of 360, 540 and 810 compared to experimental setup case of 240 mm.

This implies that there is a maximum threshold for the advantages gained from enlarging the diameter of a chimney. Beyond a specific limit, increasing the size of the chimney diameter hinders performance by causing excessive airflow dispersion. To summarize, it is essential to optimize the chimney diameter, but it is equally important to avoid an excessively large design. Effective designs must maintain a balanced chimney diameter to prevent the dilution of buoyancy-driven convection under solar heating. Proper sizing of the chimney diameter relative to the collector is key to maximizing power plant's output.

Due to the complex cyclone flow behavior, the maximum velocity at the chimney entrance (Fig. 10a) does not follow the same trends as the maximum velocity (Fig. 13) within the solar chimney system. This variation is influenced by the shape and dynamics of the cyclone flow inside the chimney.

4.3. Power and flow rate analysis

The power output of a solar chimney increases as the wind kinetic energy of the air inside the chimney rises. The wind kinetic energy ($\dot{E}$) is related to the mass flow rate ($\dot{m}$) and wind speed (V), and it can be

calculated using $\dot{E} = \frac{1}{2}\dot{m}V^2 = \frac{1}{2}\rho AV^3$. Hence, as air speed increases inside the chimney, one expects kinetic energy output to increase. The mechanical power output ($\dot{W}$) increases as wind kinetic energy ($\dot{E}$) increases, which is calculated by from mechanical efficiency of the wind turbine (η) using the following equation: $\dot{W} = \eta\dot{E}$. The percentage increase in kinetic power and mass flow rate of air with varying numbers of TPWs (3, 4, and 8) compared to a case with zero TPWs over the course of the day are shown in Fig. 14a and b, respectively. While Fig. 14c, compares the effect of percentage gained in power with number of TPWs. Fig. 14a, which illustrates the percentage gain in power, reveals a significant increase as the number of TPWs rises. The configuration with 8 TPWs consistently shows the highest percentage gain, with this effect being most pronounced during midday hours when solar radiation peaks. This suggests that adding TPWs significantly enhances the power output of the chimney, as they help organize the air flow and reduce undesirable mixing, leading to a stronger swirl flow inside the chimney. Fig. 14b, which depicts the percentage gain in mass flow rate, shows a similar trend. The configuration with 8 TPWs achieves the highest percentage gain, followed by 4 TPWs and 3 TPWs. However, the increase in mass flow rate is less pronounced compared to the corresponding increase in power. These results collectively demonstrate that increasing the number of TPWs improves both the power output and the mass flow rate in SCPP, highlighting the importance of optimizing the number of TPWs for maximum efficiency in harnessing solar energy.

Fig. 15 illustrates the impact of chimney diameter (360 mm, 540 mm, and 810 mm) on the percentage of gained power and mass flow rate compared to a baseline diameter of 240 mm. A larger chimney diameter significantly enhances both metrics, with the 810 mm chimney achieving the highest performance. Power gains peak at nearly 300 % during midday for the 810 mm diameter, while the 540 mm and 360 mm diameters reach around 150–200 % and 50–100 %, respectively. Similarly, mass flow rate gains are most pronounced for the 810 mm diameter, exceeding 800 % consistently throughout the day, followed by 400–500 % for 540 mm and 100–200 % for 360 mm. These results demonstrate that increasing the chimney diameter improves cyclone formation, reduces friction losses and enhances airflow capacity, leading to substantial improvements in system efficiency and energy output, with the 810 mm diameter being the most effective option for optimal performance.

Therefore, as the chimney diameter increases, both power output and mass flow rate significantly improve, likely due to stronger updraft and increased air flow. In the context of the present results and in line with previous large-scale designs, the optimal diameter strikes a balance between performance gains [15] and the increased construction costs and structural challenges. Further research is needed to explore the impact of other factors, such as chimney height, collector area, and geographic location, on SC performance.

5. Conclusion

Given the assumptions the current study presents a 3D CFD simulation using FLUENT of a small-scale exiting prototype. The numerical results are validated with the experimental results of exiting prototype, with an average error of 6.68 % and 9.35 % in velocity and temperature distribution. A typical use of TWPs is analyzed for enhancement in overall performance. In all configurations investigated, a peak in overall performance is observed at 1PM, the period of maximum sunshine. Further, the overall performance is analyzed in the similar fashion for different diameters. The following are the conclusions for TPWs and diameter effect.

- With an introduction of TPWs, an induced swirling flow results in an enhancement of velocity at chimney's entrance. 55.6 % and 27.87 % improvement in air velocity and temperature were recorded with use of 8 TPWs, respectively. For a day round operation, the average percentage gain in power output was observed between 40 and 330.83 %, while for mass flow rate between 103.83 % to 140 %, treating the solar chimney with zero TPWs as reference.
- With increasing diameter of chimney, a consistent enhancement in mass flow rate, while a controversial degradation in average temperature and velocity was observed. The case of chimneys diameter as 810 mm results in 87 % enhancement in flow rate and 45.28 % degradation in average temperature over 240 mm. The overall performance in terms of gained power increases with chimney diameter and varies from 83.67 % to 250 %, while the percentage gain in mass flow rate varies from 195 % to 885 %, treating the solar chimney with diameter of 240 mm as reference.

The increase in velocity due to TPWs is attributed to the induced swirling motion of air, resulting in generation of stronger and coherent updraft and elimination of re-circulation zones, while increase in chimney diameter broadens the velocity distribution. The difference in the velocity and mass flow rate distribution under varying diameter is attributed to complex dynamics of cyclonic behavior near the entrance. A future scope of modelling TPWs solar chimney in association with the ground effect, loading conditions and addressing the swirl dynamics more in depth exit in good health. A typical design leaves a potential room for its practical implication in natural ventilation system for indoor and outdoor applications, solar-driven ventilation for agricultural greenhouses and green buildings.

CRediT authorship contribution statement

Muhammad Ahmad: Writing – original draft, Validation, Investigation, Formal analysis, Conceptualization. **Siddique Mohd Umair:** Writing – review & editing, Methodology, Conceptualization. **Mohammad O. Hamdan:** Writing – review & editing, Supervision, Project administration, Investigation, Funding acquisition, Conceptualization.

Declaration of competing interest

The authors declare that they have no known competing financial interests or personal relationships that could have appeared to influence the work reported in this paper.

Acknowledgements

The authors express their gratitude to the American University of Sharjah for the research support extended through Grant No. FRG23-C-E18 and OPFY25-3152-O E 2571. The views expressed in this paper are those of the authors and do not necessarily represent the official stance of the American University of Sharjah.

Data availability

Data will be made available on request.

References

[1] A.M. Salim, I. Alsyouf, Renewable energy in the United Arab Emirates: status and potential, in: 2020 Advances in Science and Engineering Technology International Conferences (ASET), 2020, pp. 1–5.
[2] U.N. Kayani, A.F. Aysan, U. Iqbal, M. Arif, I.U. Rehman, Foreign Direct Investment Settlement, Novel Energy Methods and CO2 Emissions: Evidence From United Arab Emirates, 12, EconJournals, 2022, p. 364.
[3] J.P. Painuly, N. Wohlgemuth, Chapter 18 - renewable energy technologies: barriers and policy implications, in: J. Ren (Ed.), Renewable-Energy-Driven Future, Academic Press, 2021, pp. 539–562.
[4] J. Schlaich, R. Bergermann, W. Schiel, G. Weinrebe, Sustainable electricity generation with solar updraft towers, Struct. Eng. Int. 14 (2004) 225–229.
[5] W. Haaf, Solar chimneys: part ii: preliminary test results from the Manzanares pilot plant, Int. J. Sustain. Energy 2 (1984) 141–161.

[6] N. Monghasemi, A. Vadiee, A review of solar chimney integrated systems for space heating and cooling application, Renew. Sustain. Energy Rev. 81 (2018) 2714–2730.
[7] H. Sharon, A detailed review on sole and hybrid solar chimney based sustainable ventilation, power generation, and potable water production systems, Energy Nexus 10 (2023) 100184. June 2023.
[8] S.K. Patel, D. Prasad, M.R. Ahmed, Computational studies on the effect of geometric parameters on the performance of a solar chimney power plant, Energy Convers. Manag. 77 (2014) 424–431. January 2014.
[9] E.S. Nia, M. Ghazikhani, Numerical investigation on heat transfer characteristics amelioration of a solar chimney power plant through passive flow control approach, Energy Convers. Manag. 105 (2015) 588–595, 15 November 2015.
[10] E. Cuce, H. Sen, P.M. Cuce, Numerical performance modelling of solar chimney power plants: influence of chimney height for a pilot plant in Manzanares, Spain, Sustain. Energy Technol. Assess. 39 (2020) 100704.
[11] A. Kasaeian, S. Molana, K. Rahmani, D. Wen, A review on solar chimney systems, Renew. Sustain. Energy Rev. 67 (2017) 954–987.
[12] N. Pasumarthi, S. Sherif, Experimental and theoretical performance of a demonstration solar chimney model—part II: experimental and theoretical results and economic analysis, Int. J. Energy Res. 22 (1998) 443–461.
[13] M.A. dos Santos Bernardes, R. Molina Valle, M.F.-B. Cortez, Numerical analysis of natural laminar convection in a radial solar heater, Int. J. Therm. Sci. 38 (1999) 42–50. January 1999.
[14] Y.J. Dai, H.B. Huang, R.Z. Wang, Case study of solar chimney power plants in northwestern regions of China, Renew. Energy 28 (2003) 1295–1304. July 2003.
[15] J.P. Pretorius, Optimization and Control of a Large-Scale Solar Chimney Power Plant, Stellenbosch: University of Stellenbosch, 2007.
[16] A.R. Shahreza, H. Imani, Experimental and numerical investigation on an innovative solar chimney, Energy Convers. Manag. 95 (2015) 446–452, 1 May 2015.
[17] W. Haaf, Solar chimneys, Int. J. Sol. Energy 2 (1984) 141–161, 01/01.
[18] L.B. Mullett, The solar chimney—overall efficiency, design and performance, Int. J. Ambient Energy 8 (1987) 35–40, 01/01.
[19] X. Zhou, J. Yang, B. Xiao, G. Hou, F. Xing, Analysis of chimney height for solar chimney power plant, Appl. Therm. Eng. 29 (2009) 178–185. January 2009.
[20] Y.J. Choi, D.H. Kam, Y.W. Park, Y.H. Jeong, Development of analytical model for solar chimney power plant with and without water storage system, Energy 112 (2016) 200–207.
[21] F. Cao, H. Li, Q. Ma, L. Zhao, Design and simulation of a geothermal–solar combined chimney power plant, Energy Convers. Manag. 84 (2014) 186–195.
[22] M. Tingzhen, L. Wei, X. Guoling, X. Yanbin, G. Xuhu, P. Yuan, Numerical simulation of the solar chimney power plant systems coupled with turbine, Renew. Energy 33 (2008) 897–905, 2008/05/01/.
[23] S. Hu, D.Y. Leung, M.Z. Chen, J.C. Chan, Effect of guide wall on the potential of a solar chimney power plant, Renew. Energy 96 (2016) 209–219.
[24] C.F. Kirstein and T.W. von Backström, "Flow through a solar chimney power plant collector-to-chimney transition section," 2006.
[25] A.M. Elsayed, O.A. Gaheen, M.A. Aziz, Enhancing solar chimney power plant performance through innovative collector curved-guide vanes configurations, Renew. Energy 232 (2024) 121127.
[26] T. Ming, Y. Wu, R.K. de_Richter, W. Liu, S.A. Sherif, Solar updraft power plant system: a brief review and a case study on a new system with radial partition walls in its collector, Renew. Sustain. Energy Rev. 69 (2017) 472–487, 2017/03/01/.
[27] R. Prasad, M.R. Ahmed, Experimental evaluation of the performance and power output enhancement of a divergent solar chimney power plant by increasing the chimney height, Front. Energy Res. 11 (2024) 1283818.
[28] P.M. Cuce, E. Cuce, D.K. Mandal, D.K. Gayen, M. Asif, A. Bouabidi, et al., ANN and CFD driven research on main performance characteristics of solar chimney power plants: impact of chimney and collector angle, Case Stud. Therm. Eng. 60 (2024) 104568.
[29] E. Cuce, Divergent chimney and sloping collector design for ground heat source integrated solar chimney power plants, J. Therm. Anal. Calorim. (2024) 1–15.
[30] P.M. Cuce, A. Saxena, E. Cuce, K.J. Kontoleon, E.K. Oztekin, S. Shaik, et al., Thermal and energy analysis of a novel solar updraft tower design with divergent chimney and convergent collector concept: CFD analysis with experimental validation, Int. J. Low-Carbon Technol. 19 (2024) 714–722.
[31] R. Natarajan, S. Yaknesh, K. Prakash, M. Al Awadh, Q.M. Al-Mdallal, Parametric optimization of flow in a solar chimney power plant under variable semi elliptical constraints, Sci. Rep. 15 (2025) 331.
[32] M.O. Hamdan, S. Khashan, Numerical investigation of Solar Chimney power plant in UAE, in: ICREGA'14-Renewable Energy: Generation and Applications, 2014, pp. 513–524.
[33] M.O. Hamdan, Analysis of a solar chimney power plant in the Arabian Gulf region, Renew. Energy 36 (2011) 2593–2598.
[34] M.O. Hamdan, O. Rabbata, Experimental solar chimney data with analytical model prediction, in: World Renewable Energy Forum, WREF 2012, Including World Renewable Energy Congress XII and Colorado Renewable Energy Society (CRES) Annual Conference, 2012, pp. 327–332.
[35] J.P. Pretorius, D.G. Kröger, Critical evaluation of solar chimney power plant performance, Sol. Energy 80 (2006) 535–544, 2006/05/01/.
[36] A. Koonsrisuk, Mathematical modeling of sloped solar chimney power plants, Energy 47 (2012) 582–589. November 2012.
[37] M. Arzpeyma, S. Mekhilef, K.M.S. Newaz, B. Horan, M. Seyedmahmoudian, N. Akram, et al., Numerical simulation of the effect of chimney configuration on the performance of a solar chimney power plant, J. Therm. Anal. Calorim. (2022) 1–15.
[38] T. Ming, W. Liu, Y. Pan, G. Xu, Numerical analysis of flow and heat transfer characteristics in solar chimney power plants with energy storage layer, Energy Convers. Manag. 49 (2008) 2872–2879, 2008/10/01/.
[39] T.-H. Shih, W.W. Liou, A. Shabbir, Z. Yang, J. Zhu, A new k-ϵ eddy viscosity model for high reynolds number turbulent flows, Comput. Fluids 24 (1995) 227–238.
[40] H.F. Fasel, F. Meng, E. Shams, A. Gross, CFD analysis for solar chimney power plants, Sol. Energy 98 (2013) 12–22.